

# Nuclear spin symmetry conservation and relaxation of water ( $\text{H}_2^{16}\text{O}$ ) seeded in supersonic jets of argon and oxygen: measurements by cavity ring-down laser spectroscopy

Carine Manca Tanner, Martin Quack and David Schmidiger

Laboratorium für Physikalische Chemie, ETH Zürich, Zürich, Switzerland

## ABSTRACT

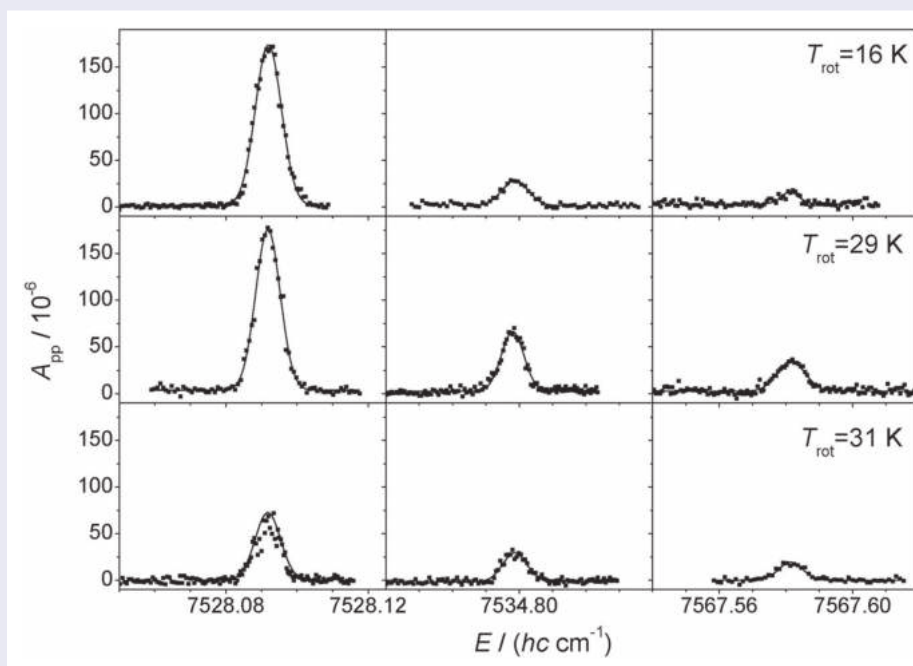
We have investigated nuclear spin symmetry conservation and relaxation of water seeded in argon or molecular oxygen using supersonic jet expansions probed by high-resolution continuous-wave laser cavity ring-down spectroscopy. The probing of the R-branch of the  $2\nu_3$  band (above  $7500\text{ cm}^{-1}$ ) was used to complement our previous investigation. We were able to further cool down the water samples (down to 17 K, i.e. 7 K colder than before) and double the data set (regarding argon as carrier gas). We confirm our first observations: at the lowest rotational temperatures and low partial pressures of  $\text{H}_2\text{O}$ , nuclear spin symmetry is conserved, in agreement with theoretical expectation for inelastic collisions. For high concentrations of water in the gas mixture, we obtained higher rotational temperatures and were able to observe nuclear spin symmetry relaxation. This can be related to the formation of water clusters at the early stage of the supersonic jet expansion. We also present the analogous series of measurements performed using molecular oxygen ( $\text{O}_2$ ) as carrier gas: we observed similar behaviour for low and high concentrations of water in the gas mixtures when cooling the samples to 16 K. The conservation of nuclear spin symmetry at low temperature and low concentration using oxygen as carrier gas indicates that the paramagnetic collisional partner does not play a significant role regarding the possible nuclear spin symmetry conversion of water. We discuss possible mechanisms related to our observations of apparent nuclear spin symmetry relaxation.

## ARTICLE HISTORY

Received 8 May 2018  
Accepted 17 May 2018

## KEYWORDS

Water ( $\text{H}_2\text{O}$ ); nuclear spin symmetry conservation; supersonic jets; high-resolution infrared spectroscopy; cavity ring-down spectroscopy



## 1. Introduction

Water, like the hydrogen molecule because of the two equivalent protons, has two nuclear spin isomers, the so-called ortho (with total nuclear spin  $I=1$ ) and para (with  $I=0$ ). While the conversion from one nuclear spin isomer to the other in the case of hydrogen molecule has been successfully performed in 1929 [1], it has been observed for the first time in 1962 in the case of water when suspended in solid Argon [2]. In a historical context, we may mention here also the early theoretical work 30 years prior to the first experimental observation [3–5].

More recently, there were claims that the ortho and para isomers of water could be separated and kept stable for a quite long time when water is adsorbed on charcoal [6]. The applications of this would be promising, for instance, for magnetic resonance imaging with the possible use of enriched water. Another interesting aspect is related to astrophysics, since the intensity of water lines is used to determine the temperature of interplanetary and interstellar objects [7–13]. Hence, the work of Tikhonov and Volkov has reactivated the interest of investigations of nuclear spin symmetry conversion for water. However, attempts to reproduce these results under similar conditions failed in several groups [14–16]. More generally, the nuclear spin symmetry conversion for water can be observed in the condensed phase [2]. This has been newly and thoroughly investigated when water is trapped in cryogenic matrices with different buffer gases and also in the presence of  $O_2$  [17–21]. Indeed, it is well known that the nuclear spin symmetry conversion is often faster in the presence of  $O_2$ . This is related to the steep magnetic field gradient produced by the collision partner  $O_2$  ( $^3\Sigma_g^-$ ), which perturbs the energy levels of the ortho and para isomers of water. The phenomenon has been investigated for  $H_2$  and  $CH_3F$  [22,23]. Regarding  $H_2O$ , Veber *et al.* [15] have estimated the rate of conversion by comparison with  $H_2$  and conclude that the pressure of  $O_2$  should be 35 Torr to get a lifetime of 1 h of a nuclear spin isomer of  $H_2O$  in the gas phase at room temperature.

Also Limbach *et al.* [24] have proposed a mechanism of ortho–para conversion when water is adsorbed on ice, analogous to  $H_2$ . When the water molecule is chemisorbed, the hydrogen bonding creates a barrier to rotation and quenches the energy levels, rendering the conversion possible if the residence time on the surface is long enough.

In the gas phase as well, nuclear spin symmetry conversion has been observed for polyatomic molecules. The mechanism assumed in this case is the so-called quantum relaxation [25]. It relies on two conditions: The first requires that two levels of energy of different nuclear spin symmetry lie close enough in order to mix. The

second imposes sufficient inelastic collisions with the environment to populate these energy levels.

Recent calculations [26] have shown that the hyperfine nuclear spin-rotational coupling constants for  $H_2O$  are small (about 30 kHz). No pair of close lying ortho–para states (separated by less than  $0.1\text{ cm}^{-1}$ ) can be found below  $3300\text{ cm}^{-1}$  and higher levels are essentially not populated under the standard experimental conditions of a supersonic expansion. This explains why at low concentration of water in an argon expansion, we could not observe any nuclear spin symmetry conversion [27,28]. At higher concentration of  $H_2O$  however, we found evidence for nuclear spin symmetry relaxation (i.e. conversion towards an equilibrium population of the nuclear spin isomers). Such a nuclear spin symmetry conversion is possible if a reactive exchange of protons (or H atoms) is possible in collisions or larger clusters, similar to processes in the liquid, although some selection rules survive even in reactive processes [29]. In the present work, we report further results regarding nuclear spin symmetry conservation and relaxation of water seeded in argon supersonic expansion, obtained with a new nozzle. These results complement and confirm our first series of experiments [27,28]. They are also used as benchmark results for a similar series of measurements using oxygen as carrier gas. The idea is to investigate whether the paramagnetic collision partner can favour any nuclear spin symmetry relaxation at low temperature and low concentration. No such enhancement of the nuclear spin symmetry conversion was found under the conditions of our experiments. Some preliminary results of our work with a coexpansion of  $H_2O$  with  $O_2$  had already been mentioned in [28] and discussed in [30]. After the present experiments had been completed, some further results were reported recently, which confirm our observations of nuclear spin symmetry conservation but could not achieve the conditions necessary for observing nuclear spin symmetry relaxation [31]. These used an experimental setup with high-resolution Fourier-transform infrared (FTIR) spectroscopy of supersonic jets similar to the one originally developed in our group for studies of nuclear spin symmetry conservation [32,33] as also later, notably in the group of Michel Herman [34–38] and we shall discuss some of the differences in the FTIR and laser spectroscopic experiments as well.

## 2. Experiment and analysis

### 2.1. Experimental setup

The jet/Cavity Ring-Down (CRD) laser spectroscopy setup combines continuous-wave CRD laser spectroscopy

with a supersonic jet expansion and has been described in detail previously [39] (see also [27,28,33,40–44]). This makes it possible to cool down and isolate the samples before probing them with high-resolution spectroscopy and with a high sensitivity. In the following, we briefly describe the main components for completeness.

A near-infrared InGaAsP laser diode (Radians Innova) emits up to about 1 mW between  $7510$  and  $8000\text{ cm}^{-1}$  in a single-frequency mode. The main part of the laser output is led through an Acousto-Optical Modulator (AOM; Isomet 1205C-2); the first-order deflection is transferred through a single-mode optical fibre and coupled into an optical cavity composed of two highly reflective concave mirrors with 1 m radius (Newport,  $R > 99.97\%$ ) mounted on an optical bench (Newport mirror holders and Spindler and Hoyer, Mikrobank) at a distance of about 33 cm.

The cavity is set up in a vacuum chamber, the vacuum being maintained by an oil diffusion pump backed by a combination of a vacuum blower pump and a mechanical roughing pump. The absorption path is crossed at right angle by a supersonic jet produced by a pulsed slit nozzle. In the present work, we used two different nozzles: (i) a  $33 \times 0.1\text{ mm}^2$  slit of the solenoid pulsed nozzle is aligned along the optical axis of the cavity and has a probe distance of less than 1 cm to the axis, and (ii) a  $40 \times 0.1\text{ mm}^2$  slit nozzle has a modified design with a variable probe distance regarding to the optical axis (between about 0.2 cm to several cm). Figure 1 shows a scheme of the two nozzles for comparison. The differences between the two setups have already been discussed [39]. Some points are worth to be recalled. Briefly, in the latter version of the nozzle, the slit has been lengthened (40 mm compared to 33 mm), the connection to the reservoir has been enlarged ensuring that the reservoir will be sufficiently filled for long openings of the valve, and the nozzle shape has been slightly modified; the slit is no longer flat on the inside of the nozzle but has a kind of conical shape as in the case of a Laval nozzle, which is expected to increase the number of collisions at the early stage of the expansion and, therefore, produce a colder sample. This new construction also makes it possible to change the probe distance between the nozzle and the optical axis of the cavity. A first series of measurements with methane has shown that (i) the  $40 \times 0.1\text{ mm}^2$  nozzle produces narrower pulses than the  $33 \times 0.1\text{ mm}^2$  nozzle and that (ii) it makes it possible to record spectra at lower temperatures [39].

When a resonance occurs in the cavity, the laser output is switched via the AOM, and the transmitted decaying light intensity is detected by a fast InGaAs photodiode (NewFocus, 125 MHz). An elaborate timing and trigger scheme allows the cavity length to match the

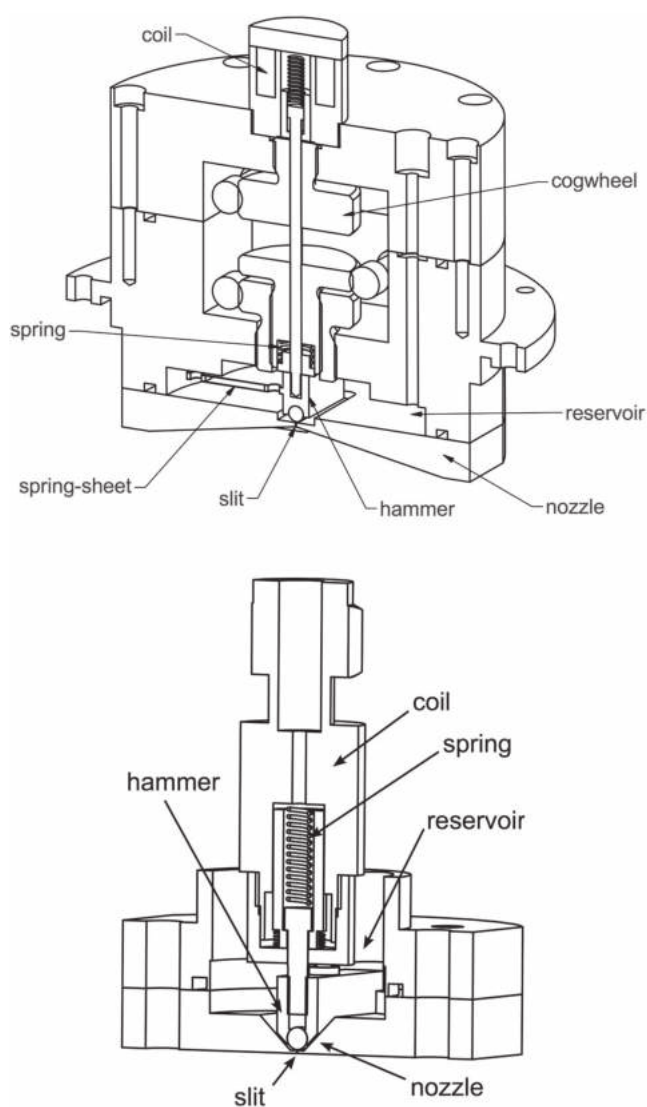


**Figure 1.** Schemes of the two nozzles used for this work: (top) the  $33 \times 0.1\text{ mm}^2$  nozzle and (bottom) the  $40 \times 0.1\text{ mm}^2$  nozzle.

laser wavelength during the gas expansion in the cavity and has been described in detail previously [39]. It also makes it possible to (i) overlap the laser beam and the gas expansion in space and time and to (ii) collect and sort resonances, depending on whether the nozzle has been activated (signal with gas expansion) or not (background).

Each recorded decay is analysed and fitted to estimate the Ring-Down (RD) constant  $k_{\text{RD}} = \tau_{\text{RD}}^{-1}$  according to:

$$I(t) = I(t=0) \exp(-t/\tau_{\text{RD}}) = I(t=0) \exp(-k_{\text{RD}}t) \quad (1)$$

where  $I(t)$  is the intensity of the transmitted light through the cavity at time  $t$ . More details of the mathematical treatment of the exponential fit are given in Reference [39].

For the results shown in this paper, between 32 and 50 decays are accumulated for resonances with the gas expansion for the ‘signal’ and between 256 and 600 for the ‘background’ (without the expansion); the two series of  $k_{RD}$  are averaged and the difference of the two averaged  $\bar{k}_{RD}$  values constitute one point of a CRD spectrum which is obtained by scanning the laser wavelength. The latter is measured at each data acquisition point with the wavemeter. For a relative calibration, the etalon fringes of a 500 MHz etalon are recorded simultaneously and used to linearise the spectrum (the free spectral range of the etalon is known with great precision, and the frequency drift is 1 MHz per day). The difference of  $\bar{k}_{RD}$  for ‘signal’ and ‘background’ is directly proportional to the absorption  $\alpha$ . The laser bandwidth is less than 1 MHz and thus the effective ‘instrumental resolution’ of the experiment is essentially determined by the frequency distance between measurement frequencies (less than 20 MHz, much less than the typical Doppler widths in our experiments of about 180 MHz or  $0.006 \text{ cm}^{-1}$ ).

## 2.2. Measurements

In a first series of measurements using the  $33 \times 0.1 \text{ mm}^2$  nozzle, we chose not to change the gas expansion parameters (i.e. nozzle time opening, delay between the nozzle opening and the laser, pressure of the gas mixture before the expansion and dynamical pressure in the cavity) so that the spectra were always recorded under the same conditions. The only parameter that was changed between two measurements was the composition of the gas mixture and more specifically the concentration of water. The gas composition was generated by sending the carrier gas through a bubbler filled with distilled water and maintained at  $\theta_{\text{bath}}$ . The same protocol was used

for two carrier gas: Argon (Ar) and Oxygen ( $\text{O}_2$ ). These results have been discussed previously in the case of Ar as carrier gas and are recalled here for comparison [27,28].

In order to confirm our first results and to enlarge the domain of temperature probed, new series of measurements were performed with both carrier gases using the  $40 \times 0.1 \text{ mm}^2$  nozzle. In this case, not only the temperature of the bubbler ( $\theta_{\text{bath}}$ ) was changed between the two measurements, but also several distances between the nozzle and the optical path were used to obtain expansions under different conditions. Tables 1 and 2 list the experimental conditions used for our measurements, including the probe distance from the nozzle to the optical axis as well as  $\theta_{\text{bath}}$  and therefore the expected partial pressure and mole fraction of water in the gas mixture depending on the partial pressure of the carrier gas (between 0.5 bar and 2 bar) before the expansion.

## 2.3. Investigation of nuclear spin symmetry conservation or relaxation

This approach has already been described in detail previously [28,32]. The key steps are briefly recapitulated here.

Our analysis of the rotational temperature and of the ortho/para ratio of the water monomer is based on the fact that the integrated absorption cross section  $G$  of the  $J'_{K'_a, K'_c} \leftarrow J_{K_a, K_c}$  transition is proportional to the population  $p$  of the initial state  $J_{K_a, K_c}$ :

$$\begin{aligned} G(J'_{K'_a, K'_c} \leftarrow J_{K_a, K_c}, \Gamma_{\text{ns}}, T_{\text{rot}}) &= \int_{\text{line}} \sigma(T_{\text{rot}}, \tilde{\nu}) \tilde{\nu}^{-1} d\tilde{\nu} \\ &\propto p(J_{K_a, K_c}, \Gamma_{\text{ns}}, T_{\text{rot}}) A(J_{K_a, K_c}, J'_{K'_a, K'_c}), \end{aligned} \quad (2)$$

**Table 1.** Experimental conditions ( $\theta_{\text{bath}}$ , estimated  $p(\text{H}_2\text{O})$ ,  $x_{\text{H}_2\text{O}}$ , nozzle dimensions and  $d$ , distance from the nozzle) used for our series of experiments with  $\text{H}_2\text{O}:\text{Ar}$  supersonic jet expansion and rotational temperature  $T_{\text{rot}}$  obtained from the ratios of integrated absorption cross sections.

$\theta_{\text{bath}}$ ( $^{\circ}\text{C}$ )	$p(\text{H}_2\text{O})$ (mbar)	$x_{\text{H}_2\text{O}}$ (%)	nozzle dimensions ( $\text{mm}^2$ )	$d$ (mm)	$G_{1,1}/G_{1,0}$	$G_{2,2}/G_{1,0}$	$T_{\text{rot}}$ (K)
2.0 (1)	7.06 (7)	0.35	$33 \times 0.1$		0.23 (2)	0.10 (2)	19 (1)
5.0 (1)	8.72 (8)	0.44	$33 \times 0.1$		0.31 (2)	0.11 (2)	22 (1)
10.0 (1)	12.27 (14)	0.61	$33 \times 0.1$		0.27 (2)	0.11 (2)	21 (1)
14.0 (1)	15.98 (13)	0.80	$33 \times 0.1$		0.30 (3)	0.14 (3)	23 (1)
16.0 (1)	18.17 (17)	0.91	$33 \times 0.1$		0.50 (4)	0.16 (2)	25 (1)
20.0 (1)	23.37	1.2	$33 \times 0.1$		0.46 (3)	0.21 (3)	27 (1)
20.0 (1)	23.37	1.2	$33 \times 0.1$		0.43 (3)	0.22 (3)	29 (1)
25.0 (1)	31.66	1.6	$33 \times 0.1$		0.43 (5)	0.25 (3)	31 (1)
15.3 (1)	17.42	3.5	$40 \times 0.1$	10	0.21 (2)	0.07	17 (1)
15.6 (1)	17.76	3.6	$40 \times 0.1$	2	0.30 (2)	0.10 (1)	22 (1)
15.6 (1)	17.76	3.6	$40 \times 0.1$	4	0.29 (2)	0.07 (1)	20 (1)
15.6 (1)	17.76	3.6	$40 \times 0.1$	6	0.27 (2)	0.06 (1)	19 (1)
15.6 (1)	17.76	3.6	$40 \times 0.1$	5	0.44	0.17	25
19.7 (1)	23.00	4.6	$40 \times 0.1$	5	0.32 (3)	0.16 (2)	24
30.6 (2)	44.15	8.8	$40 \times 0.1$	5	0.39 (2)	0.26 (2)	32
23.4 (2)	28.83	5.8	$40 \times 0.1$	5	0.38 (5)	0.16 (2)	25

Note: Numbers in parentheses provide uncertainties in units of the last digits given. For the  $33 \times 0.1 \text{ mm}^2$  nozzle  $d$  is less than 10 mm and not variable.

**Table 2.** Experimental conditions ( $\theta_{\text{bath}}$ , estimated  $p(\text{H}_2\text{O})$ ,  $x_{\text{H}_2\text{O}}$ , nozzle dimensions and  $d$  distance from the nozzle) used for our series of experiments with  $\text{H}_2\text{O}:\text{O}_2$  supersonic jet expansion, and rotational temperature  $T_{\text{rot}}$  obtained from the ratios of integrated absorption cross sections.

$\theta_{\text{bath}}$ ( $^{\circ}\text{C}$ )	$p(\text{H}_2\text{O})$ (mbar)	$x_{\text{H}_2\text{O}}$ (%)	nozzle dimensions ( $\text{mm}^2$ )	$d$ (mm)	$G_{1,1}/G_{1,0}$	$G_{2,2}/G_{1,0}$	$T_{\text{rot}}$ (K)
20 (1)	23.37	1.2	$33 \times 10$		0.42 (6)	0.35 (5)	38
20 (1)	23.37	1.2	$33 \times 0.1$		0.39 (3)	0.30 (2)	35
10 (1)	12.27	0.6	$33 \times 0.1$		0.34 (3)	0.27 (2)	32
4.5 (1)	8.45	1.7	$40 \times 0.1$	2	0.36 (2)	0.23 (1)	29
10 (1)	12.27	0.6	$33 \times 0.1$		0.31 (4)	0.16 (7)	25
10.3 (1)	12.57	2.5	$40 \times 0.1$	6	0.3 (2)	0.15 (2)	24
5.8 (2)	9.23	1.8	$40 \times 0.1$	2	0.32 (2)	0.14 (2)	23
3.5 (1)	7.88	1.6	$40 \times 0.1$	6	0.31 (1)	0.1 (2)	21
7.4 (1)	10.31	2.1	$40 \times 0.1$	6	0.24 (1)	0.08 (2)	18
2.5 (2)	7.34	1.5	$40 \times 0.1$	2	0.17 (2)	0.05 (1)	16
10 (1)	12.27	1.8	$40 \times 0.1$	2	0.30 (3)	0.12 (2)	22
23 (1)	28.0	4.0	$40 \times 0.1$	6	0.43 (3)	0.25 (2)	31

Note: Numbers in parentheses provide uncertainties in units of the last digits given. For the  $33 \times 0.1 \text{ mm}^2$  nozzle  $d$  is less than 10 mm and not variable.

$\sigma(T_{\text{rot}}, \tilde{\nu})$  is the effective absorption cross section and  $A(J_{K_a, K_c}, J'_{K'_a, K'_c})$  is the rotational line strength factor for the  $J'_{K'_a, K'_c} \leftarrow J_{K_a, K_c}$  transition.

We assume that the populations follow a Boltzmann distribution except for nuclear spin symmetry effects. Hence, if the nuclear spin symmetry is conserved during the cooling process of the supersonic expansion, the ortho and para isomers keep their relative populations set at room temperature before the expansion and one should observe a superposition of two Boltzmann distributions, one for each nuclear spin isomer between its energy levels. On the other hand, in the case of nuclear spin symmetry relaxation, the nuclear spin states are allowed to change during the collision process of the expansion and the relative populations should represent a global thermal equilibrium among all the states at low temperature.

For a spectroscopic investigation of nuclear spin symmetry conservation or relaxation, at least three lines have to be measured in the case of water [33]: (i) at least one transition associated with each nuclear spin isomer has to be measured in order to estimate the relative populations of the isomers and (ii) at least one extra transition associated to one of the nuclear spin isomers has to be measured to determine the rotational temperature. Using a supersonic jet expansion prevents us from easily knowing the total concentration of the probed species. In recent work [28,39], we have already shown that we can circumvent this problem by working with *relative* effective integrated absorption cross section of one line compared to another assuming that the supersonic jet expansion remains uniform during a day.

In our previous work on water, we have already discussed in detail the choice of the probed transitions [28]: they are all from the R-branch of the  $2\nu_3$  band. One might think that three lines only, i.e. the minimum required, is hardly sufficient to determine the rotational temperature and furthermore to investigate the ortho/para ratio of

water monomer. Before we discuss the results regarding nuclear spin symmetry conservation or relaxation, we would like to provide some further observations in order to support our results on water.

In our most recent investigation of methane with the supersonic jet/CRD setup [39], 21 transitions of the  $\nu_2 + 2\nu_3$  band were investigated between 7 and 48 K; we have observed an excellent agreement between our experimental measurements and the predictions of temperature based on the assumption that the population follow a Boltzmann distribution as described in [32], except for nuclear spin symmetry effects. Moreover, we have changed our experimental conditions of the supersonic jet expansion between two series of measurements using a larger pressure of argon and a lower partial pressure of water compared to the measurements with methane. Therefore, the collision rate of a probed molecule with argon at 300 K increased (from about  $8 \times 10^9 \text{ s}^{-1}$  for methane, up to  $2 \times 10^{10} \text{ s}^{-1}$  for water), which should compensate for a reduced cooling efficiency of water, if any, even though unlikely. For the series of measurements with water, the rotational temperature was estimated between 19 and 31 K. Moreover, whenever possible, further lines were measured in addition to the three systematically investigated, for instance, the  $J' = 2_{K'_a=1, K'_c=2} \leftarrow J = 1_{K_a=0, K_c=1}$  transition; its effective integrated absorption cross section does not indicate any sizeable non-Boltzmann effect and confirms our estimation of the rotational temperature when this test was possible [27,28].

Finally, we estimated the transversal translational temperature of the expansion from the Full Width at Half Maximum of the lines measured using a fit with a Gaussian profile. Depending on the concentration of water in the gas mixture, we found a Doppler width ranging from  $0.0055$  to  $0.0067 \text{ cm}^{-1}$ , which corresponds to an effective translational temperature of about 22 up to 30 K, which is in good agreement with our estimation of the rotational

temperature. Here again, we found consistent behaviour: (i) the Doppler width decreases as the estimated rotational temperature decreases and (ii) the translational temperature of water is similar to that estimated in the case of the methane measurements. While the apparent translational temperature derived from the Doppler line shape need not be identical to the rotational temperature, and, indeed, the line shape need not be Gaussian, in principle, we have found that for our expansion conditions the simple relation of apparent rotational and translational temperatures is frequently satisfied, including hydrides such as HF and (HF)<sub>2</sub> and their isotopomers [40,41] and CH<sub>4</sub> [39,42]. For all these reasons, we believe that even if only three lines were used, the reproducibility of our setup and robustness of our approach is adequate as shown by our previous measurements.

Since there is no ambiguity between the transitions of the  $2\nu_3$  band investigated systematically, from now on, we use a simplified notation:  $G_{J_{K_a, K_c}}$  is the integrated absorption cross section of the transition in the R-branch originating from the state  $J_{K_a, K_c}$ . Therefore,

- $G_{1_{1,0}}$  is the integrated absorption cross section of the  $2_{2,1} \leftarrow 1_{1,0}$  transition of the ortho isomer ( $J'_{K'_a, K'_c} \leftarrow J_{K_a, K_c}$  notation),

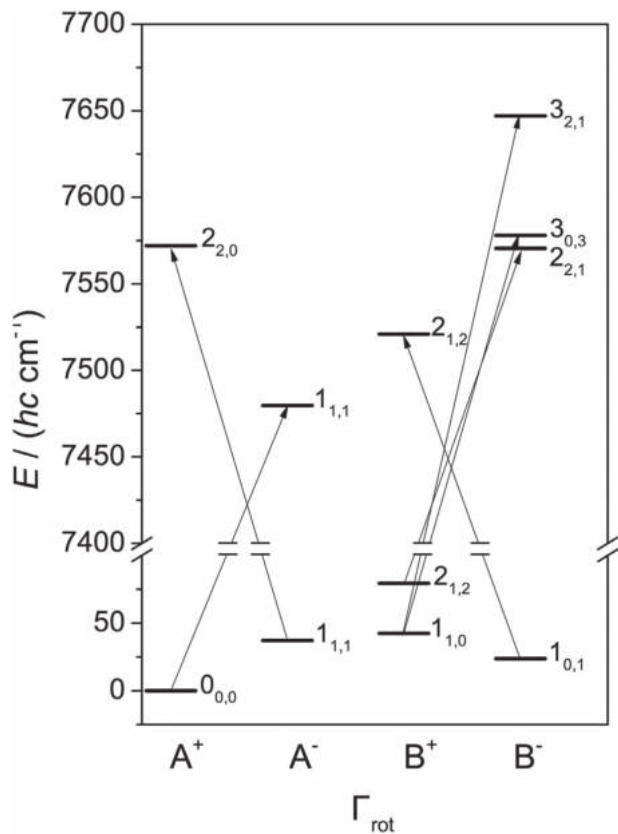


**Figure 2.** Energy levels  $J_{K_a, K_c}$  and transitions as observed in this work. The energy axis has been cut to highlight the region of the initial and final levels.

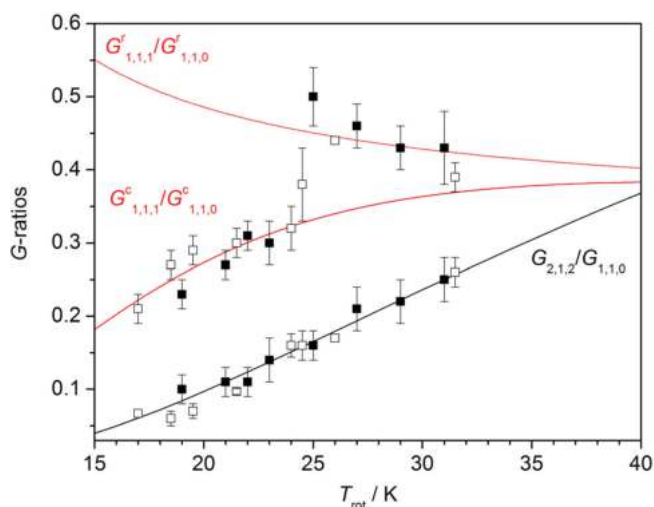
- $G_{1_{1,1}}$  is the integrated absorption cross section of the  $2_{2,0} \leftarrow 1_{1,1}$  transition of the para isomer and
- $G_{2_{1,2}}$  is the integrated absorption cross section of the  $3_{2,1} \leftarrow 2_{1,2}$  transition of the ortho isomer.

Figure 2 shows the relevant levels and transitions as observed in our work on H<sub>2</sub><sup>16</sup>O (see [28,29] for the symmetry notations).

### 3. Results

#### 3.1. Nuclear spin symmetry conservation at low concentration

Figure 3 shows the  $G$ -ratios of the R(1<sub>1,1</sub>) and R(2<sub>1,2</sub>) transitions compared to the R(1<sub>1,0</sub>) transition as a function of the rotational temperature for various H<sub>2</sub>O:Ar expansions. The full symbols correspond to measurements with the  $33 \times 0.1$  mm<sup>2</sup> nozzle and have already been discussed [27,28]. The open symbols correspond to measurements with the  $40 \times 0.1$  mm<sup>2</sup> nozzle. All experimental conditions are listed in Table 1. Globally, we observe the same kind of results with the two nozzles, the new series confirming our first observations: there is nuclear spin symmetry conservation at low temperature and low concentration of water in argon and nuclear spin symmetry relaxation at higher temperature and higher



**Figure 3.** Ratios of integrated absorption cross section ( $G$ ) of the R(1<sub>1,1</sub>) and R(2<sub>1,2</sub>) transitions compared to that of the R(1<sub>1,0</sub>) transition as a function of the rotational temperature  $T_{rot}$ . The superscripted  $c$  and  $r$  in  $G^c$  and  $G^r$  indicate that the ratios were calculated assuming nuclear spin symmetry conservation and relaxation, respectively. The uncertainty indicated for the experimental points from the various H<sub>2</sub>O:Ar expansions arises from the Gaussian fit of each line measured with the jet-CRD setup only. The full symbols correspond to measurements with the  $33 \times 0.1$  mm<sup>2</sup> nozzle, while the open symbols are for the  $40 \times 0.1$  mm<sup>2</sup> nozzle.

concentration (see discussion below). Looking into more detail, the  $40 \times 0.1 \text{ mm}^2$  nozzle makes it possible to further cool down the water samples: under similar conditions, we obtained  $T_{\text{rot}} = 24 \text{ K}$  with the  $33 \times 0.1 \text{ mm}^2$  nozzle and  $T_{\text{rot}} = 17 \text{ K}$ , 7K colder with the  $40 \times 0.1 \text{ mm}^2$  nozzle. The  $40 \times 0.1 \text{ mm}^2$  nozzle made it possible to double our data set and confirm our previous results.

As already mentioned previously [28], we performed further series of measurements using molecular oxygen  $\text{O}_2$  instead of argon as carrier gas. Figure 4 shows the

jet-CRD spectra of the three lines of water investigated using argon and oxygen as carrier gas with the  $33 \times 0.1 \text{ mm}^2$  nozzle, all other parameters of the expansion being the same. As expected, the collisional cooling is more efficient with argon than with oxygen: the lines appear broader in the case of oxygen and the rotational temperature has been estimated to be 38 K, 9 K higher than in the case of argon. Figure 5 shows the spectra recorded in a second series of measurements using the  $40 \times 0.1 \text{ mm}^2$  nozzle. As in the case of argon, we

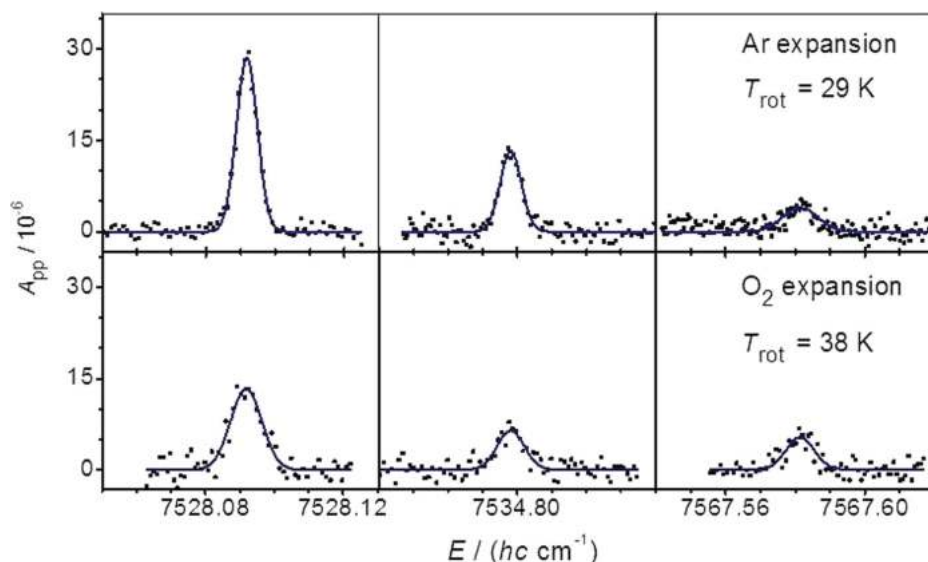


**Figure 4.** Jet-CRD spectra as absorbance per pass  $A_{\text{pp}}$  of the  $\text{R}(1_{1,0})$ ,  $\text{R}(1_{1,1})$  and  $\text{R}(2_{1,2})$  transitions of water for a  $\text{H}_2\text{O}:\text{Ar}$  (top) and  $\text{H}_2\text{O}:\text{O}_2$  (bottom) gas mixture with  $x_{\text{H}_2\text{O}} = 1.2\%$ .

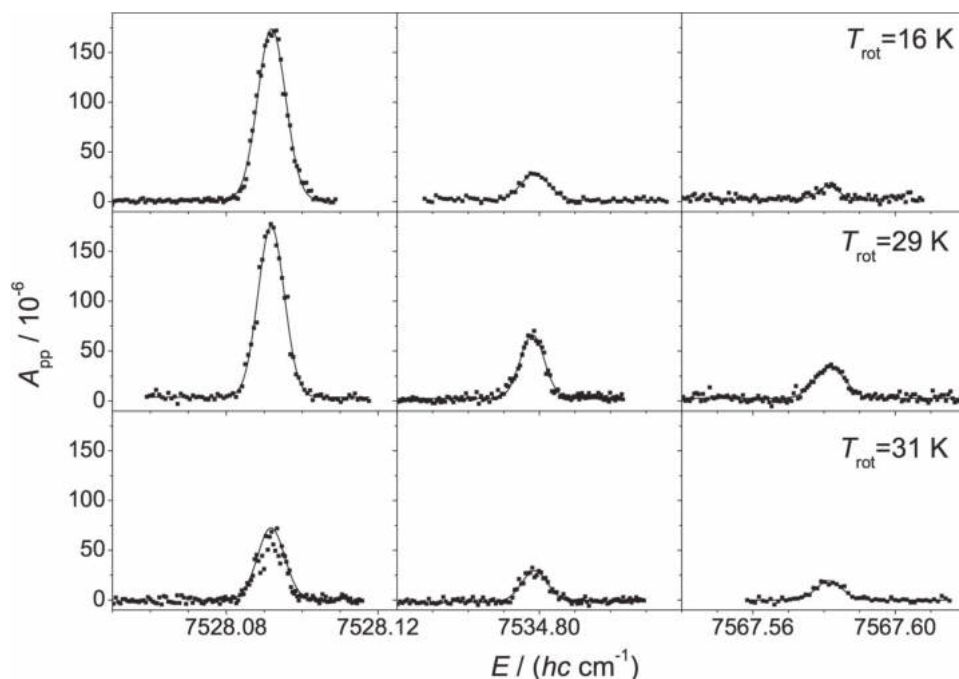


**Figure 5.** Jet-CRD spectra as absorbance per pass  $A_{\text{pp}}$  of the  $\text{R}(1_{1,0})$ ,  $\text{R}(1_{1,1})$  and  $\text{R}(2_{1,2})$  transitions of water for various  $\text{H}_2\text{O}:\text{O}_2$  gas mixtures: (top)  $x_{\text{H}_2\text{O}} = 1.5\%$ , (middle)  $x_{\text{H}_2\text{O}} = 1.7\%$ , and (bottom)  $x_{\text{H}_2\text{O}} = 4.0\%$ .

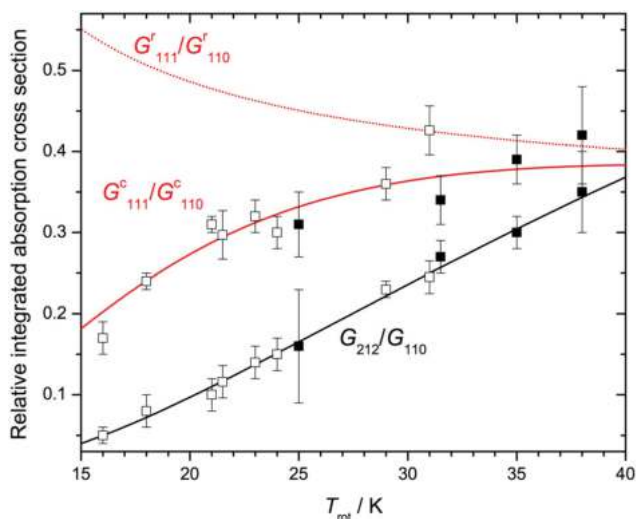


**Figure 6.** Ratios of integrated absorption cross section ( $G$ ) of the  $R(1_{1,1})$  and  $R(2_{1,2})$  transitions compared to that of the  $R(1_{1,0})$  transition as a function of the rotational temperature  $T_{\text{rot}}$ . The superscripted  $c$  and  $r$  in  $G^c$  and  $G^r$  indicate that the ratios were calculated assuming nuclear spin symmetry conservation and relaxation, respectively. The uncertainty indicated for the experimental points from the various  $\text{H}_2\text{O}:\text{O}_2$  expansions arises from the Gaussian fit of each line measured with the jet-CRD setup only. The full symbols correspond to measurements with the  $33 \times 0.1 \text{ mm}^2$  nozzle, while the open symbols correspond to measurements with the  $40 \times 0.1 \text{ mm}^2$  nozzle.

obtained the lowest temperatures with this latter nozzle when using oxygen as carrier gas. All experimental conditions are listed in Table 2. Finally, Figure 6 shows the  $G$ -ratios of the  $R(1_{1,1})$  and  $R(2_{1,2})$  transitions compared to the  $R(1_{1,0})$  transition as a function of the rotational temperature for various  $\text{H}_2\text{O}:\text{O}_2$  expansions. The full symbols correspond to measurements with the  $33 \times 0.1 \text{ mm}^2$  nozzle, while the open symbols correspond to measurements with the  $40 \times 0.1 \text{ mm}^2$  nozzle. In this case, too, we observed nuclear spin symmetry conservation at low concentration of water and low temperatures, between 16 K and 25 K (see Figure 6).

The fact that we observed the same effect for different series of measurements, using different nozzles and different carrier gases confirms our previous results as expected for low concentrations, i.e. the nuclear spin symmetry conservation of water in a supersonic expansion. This result agrees with what has been found for methane [32,39,42,45], for example and with the predictions from the theory of nuclear spin symmetry conservation in inelastic collisions [29,46–48].

### 3.2. Clusterisation-induced nuclear spin symmetry relaxation

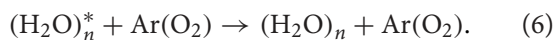
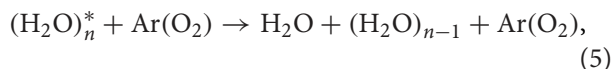
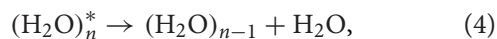
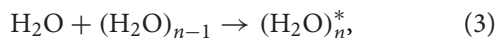
In our first series of measurements of water seeded in argon performed with the  $33 \times 0.1 \text{ mm}^2$  nozzle

[27,28], we also found experimental conditions for which we observed nuclear spin symmetry relaxation (see Figure 3). These correspond to the ‘highest’ mole fractions of water ( $x_{\text{H}_2\text{O}} > 0.9\%$ ) and the ‘highest’ temperatures. Using the  $40 \times 0.1 \text{ mm}^2$  nozzle and slightly different expansion conditions, we were also able to find a regime where we could observe nuclear spin symmetry relaxation again, confirming our first observations of this phenomenon as well.

The conclusions are a little less straightforward in the case of oxygen as carrier gas. Actually, the first series of measurements, performed with the  $33 \times 0.1 \text{ mm}^2$  nozzle was not conclusive on nuclear spin symmetry relaxation at ‘high’ concentration and ‘high’ temperatures because the error bars deduced from the line fitting were too large and overlapping both models, i.e. the nuclear spin symmetry relaxation and conservation, using the  $G$ -ratios (see Figure 6). In a second series of measurements, performed with the  $40 \times 0.1 \text{ mm}^2$  nozzle, the situation appeared first to be similar but this latter nozzle makes it possible to further cool down our samples. We actually can increase the range of temperatures probed by 10 K, from 25 K down to 15 K. On the other hand, it is more difficult to obtain ‘warmer’ expansions, say at 30 K or more. Nevertheless, we managed to obtain a few points in this region after several attempts. Since the molecular beam is significantly more stable, the estimation of  $G$ -ratios is better and the error bars are significantly smaller: we can now clearly observe nuclear spin symmetry relaxation also for water seeded in oxygen at ‘high’ temperatures and ‘high’ concentrations (4%), as in the case of water seeded in argon.

In our previous work, we have correlated the nuclear spin symmetry relaxation with the formation of water clusters  $(\text{H}_2\text{O})_n$ , or more precisely, with the decrease of the relative proportion of the water monomer in the supersonic expansion. As discussed already in [28], it is not possible to directly investigate the water clusters under our experimental conditions. The relative concentrations of water clusters in various slit-jet expansions have already been investigated by several groups under various conditions [49–51]. Work on hydrogen fluoride clusters has shown a great variety of clusters formed depending upon detailed expansion conditions, including the formation of nanoclusters [52–55]. Although we cannot conclude on the size and relative concentrations of water clusters in our experiments, we believe that there exists clear evidence for large cluster formation. Excited water clusters can be formed in a supersonic jet expansion via two-body collisions. These clusters then redissociate or the additional collisions with the carrier gas might lead to the dissociation or the stabilisation of the briefly formed clusters according to the following

simplified mechanism:



The water molecules resulting from the formation/dissociation mechanism according to reactions (3)–(5) and therefore of reaction (6) would then exhibit monomer components on the spectrum but would also retain the information of the cluster lifetime where nuclear spin symmetry change can happen according to two main mechanisms [28]:

- (i) in the *de facto* mechanism for change of nuclear spin symmetry, the nuclear spin symmetry of the monomer  $\text{H}_2\text{O}$  appearing as reactant in the collision with  $(\text{H}_2\text{O})_{n-1}$  in Equation (3) is different from the nuclear spin symmetry of the  $\text{H}_2\text{O}$  product in the dissociation of the intermediate complex  $(\text{H}_2\text{O})_n^*$  in Equation (4). This can happen when protons are exchanged between water molecules in the intermediate cluster,
- (ii) in the *de lege* mechanism for change of nuclear spin symmetry, the nuclear spin symmetries can mix in an intermediate cluster because of change of symmetry or modification of the energy level distribution. The mechanism is essentially the same as in the general quantum relaxation model for polyatomic molecules [25,56–58], the complex  $(\text{H}_2\text{O})_n$  being treated as the polyatomic molecule. Although little is known about such processes in  $(\text{H}_2\text{O})_n$ , they appear qualitatively much more likely than in the monomer  $\text{H}_2\text{O}$ , because of the much higher density of quantum states and thus higher likelihood of near degeneracies in  $(\text{H}_2\text{O})_n$ .

At the present time, our results cannot distinguish between the two mechanisms as we observe only the net effect on the monomer symmetry (ortho or para  $\text{H}_2\text{O}$ ). Nevertheless, we would like to emphasise the fact that not simply the presence of water clusters as such suffices to observe nuclear spin symmetry relaxation. It is a dynamical process which strongly depends on the experimental conditions and experimental setup, determining the size of the clusters formed, their abundance, their degree of excitation and further properties, which all have influence on kinetic processes. We were able to find conditions with our experimental setup to observe nuclear

spin symmetry relaxation but one can imagine observing water clusters and no nuclear spin symmetry relaxation of the monomer [31,59–61]. One possible reason would be that in the conditions of the expansion, very few water clusters dissociate after the formation. Hence the proportion of water monomers retaining the information of the conversion during the cluster lifetime would be very small or even negligible to observe an effect. Another possible reason would be if the *de lege* mechanism for symmetry breaking of nuclear spin symmetry is important. One can then assume that the size of the clusters, which strongly depend on the experimental setup and conditions, play a key role: the larger the clusters, the more probable the mechanism. Cluster size would also affect the *de facto* mechanisms because of different barriers for the proton exchange. As discussed before [28] even for  $n = 2$  in Equations (3) and (4), nuclear spin symmetry conversion is possible if only symmetry is considered [29] but for such small clusters barriers to exchange are presumably too high to significantly contribute to such processes.

### 3.3. Investigation on the effect of the paramagnetic moment of the collisional partner

In 1935, it was found that nuclear spin symmetry conversion from ortho to para molecular hydrogen can be induced in the gas phase by collision with a partner carrying a magnetic moment [62]. Actually molecular oxygen ( $\text{O}_2$ ) speeds up the hydrogen nuclear spin symmetry conversion by four to five orders of magnitude. On the other hand, it has been shown that the paramagnetism of  $\text{O}_2$  cannot contribute to the main mechanism behind the ortho to para conversion in the case of  $^{12}\text{CH}_3\text{F}$  and  $^{13}\text{CH}_3\text{F}$  [23,63]. The mechanism has been investigated theoretically [22,23]: the paramagnetism of  $\text{O}_2$  produces a magnetic field which can induce transitions between the energy levels of the ortho and para nuclear spin isomers of the probed system.

In order to investigate the effect of the paramagnetic  $\text{O}_2$  on the ortho–para conversion of water, we have investigated supersonic jet expansion of water seeded in molecular oxygen. This investigation is similar to that performed using argon as carrier gas. Hence, comparing the results will reveal the effect of the carrier gas and more specifically the possible role of the paramagnetism of oxygen.

As discussed above, we observed the same behaviour regarding nuclear spin symmetry conversion using either argon or oxygen as carrier gas. The nuclear spin symmetry relaxation observed at ‘high’ temperatures and ‘high’ concentrations in argon is related to the formation of water clusters. We can assume a similar mechanism

under the same experimental conditions when oxygen is used as carrier gas. Moreover, if the nuclear spin symmetry relaxation observed at high temperature and high concentration in oxygen were due to the paramagnetism of  $O_2$ , there is no reason why this mechanism should not apply also at low temperature and low concentration unless one invokes  $[(H_2O)_n(O_2)_m]$  clusters. We do not observe nuclear spin symmetry relaxation of water in  $O_2$  at low temperature and low concentration; therefore, we conclude that the paramagnetic  $O_2$  does not play a significant role in nuclear spin symmetry conversion of water under our experimental conditions, probably because there are too few collisions between water and the collision partner  $O_2$  ( $^3\Sigma_g^-$ ) in the expansion.

#### 4. Discussion and conclusions

Following our previous work using CRD spectroscopy of  $H_2O$  in supersonic jets [27,28], we have reinvestigated the nuclear spin symmetry conservation and relaxation of supersonic jet expansions of water seeded in argon and in oxygen, substantially extending the conditions. Our results fully confirm, complement and extend our first series of measurements:

- (i) Our new home-built nozzle made it possible to reach colder rotational temperatures than the previous 33 mm long nozzle (17 K. i.e. 7 K colder) and to double the amount of data.
- (ii) Effective nuclear spin symmetry conservation appears to be valid under conditions of high dilution for  $H_2O$  in Ar and in  $O_2$ . The room temperature ratio of ortho and para  $H_2O$  is essentially maintained. The nuclear spin symmetry conservation under conditions where  $H_2O$  monomer collisions with Ar dominate the cooling process is in agreement with expectations for such inelastic collisions and the short time scale of the supersonic jet expansion, including quantitative estimates for interconversion rates for nuclear spin isomers of  $H_2O$  [16,26,46–48].
- (iii) At somewhat higher concentration of  $H_2O$  in Ar or in  $O_2$ , when the formation of  $(H_2O)_n$  is possible and evident from the mass balance, we find a change of the ratio of concentrations of ortho to that of para isomers apparently relaxing to a near-Boltzmann equilibrium at the relevant low temperature in the jet. The observation of nuclear spin symmetry relaxation under conditions where  $(H_2O)_n$  clusters are present in the jet allows for interpretations of this phenomenon by different mechanisms.

- (iv) The similar behaviour observed using argon or molecular oxygen as carrier gases reveals that the paramagnetism of the collision partner in the supersonic expansion does not play a dominant role in the nuclear spin symmetry conversion of water under our experimental conditions.

While the experimental results on the population distributions observed here by high-resolution laser spectroscopy of supersonic jet expansions of  $H_2O$  are firm and (confirmed here a second time again), the interpretation in terms of nuclear spin symmetry conservation or relaxation deserves further attention, also in relation to more recent results by FTIR spectroscopy of supersonic jets of  $H_2O$  [31] in following up our earlier work [27,28], but with the claim of an opposite conclusion on relaxation. In this context, it may be suitable to first address the different techniques with their advantages and disadvantages, particularly when applied to the question of nuclear spin symmetry conservation or relaxation in supersonic jet expansion (see also the reviews [33,64]). While spectroscopic observations (at high and low resolution) of molecular beams date back to the early days of the technique (see reviews in [64–66] for instance), the spectroscopic accuracy and resolution needed to study the question of nuclear spin symmetry conservation in polyatomic molecules ( $CH_4$ ) was available originally by means of laser spectroscopy [67] (see also ref [64] for a more complete history).

A disadvantage in practice (although not in principle) of laser spectroscopy is the limited spectral range easily covered in single experiments at very high resolution. In order to overcome this disadvantage in the decade of 1980–1990, we developed high-resolution FTIR spectroscopy of supersonic jets [32,68–70]. This has not only allowed to study the question of nuclear spin symmetry conservation by spectroscopy [32] but also the formation of hydrogen-bonded clusters over a wide range of cluster size [52–55] showing absorption in a wide range of frequencies. The remaining disadvantage of lower sensitivity and resolution in FTIR spectroscopy could be overcome by combining results from high-resolution FTIR spectroscopy and high-resolution diode laser spectroscopy of supersonic jets in very similar parallel setups in our laboratory [71–73]. Notably, the group of Michel Herman has later followed a similar strategy addressing also similar questions [36,38,74,75] where one should mention in particular the elegant combination of two experiments in the same setup (FANTASIO [36]). It remains true, however, to this date, that if applied separately, each technique suffers individually from the original drawbacks, FTIR spectroscopy having more limited resolution and sensitivity, laser spectroscopy more

limited spectral coverage (at least in practice, for a recent review of both techniques as well as their combination, see [33]).

In comparing the recent experiments on  $\text{H}_2\text{O}$  nuclear spin symmetry, one finds the very high sensitivity of laser spectroscopy allowing for the study of very small absorptions and a wide range of beam and temperature conditions in [27,28] as in the present work, but without information on the cluster spectra occurring in a different spectral range. On the other hand, FTIR spectroscopy has more limited resolution and in particular sensitivity [31]. This leads to a more complex analysis of the data needing the separation of high-temperature background spectra from the actual low-temperature supersonic jet spectra, the accuracy of which is difficult to assess as well as possible, although probably less important, distortions of line intensities due to more limited resolution. On the other hand, FTIR spectra show clear evidence for the presence or absence of  $(\text{H}_2\text{O})_n$  clusters, although the resolution is insufficient to show sharp individual lines of  $(\text{H}_2\text{O})_2$ ,  $(\text{H}_2\text{O})_3$ , etc. to identify them individually. The type of nozzle used in [31] is not specified so precisely, but it seems clear that the conditions of the experiments are sufficiently different, that the nature of the clusters formed in the beams can be assumed to be quite different. Thus, the most likely interpretation of the differences in results from [27,28] and [31] is the different nature of the clusters formed and their different kinetics. Certainly, in spite of what was stated in [31] that work contains no evidence whatsoever contradicting the results in [27,28] but is simply consistent with the assumption that the clustering condition achieved in [27,28] and in the present work could not be reached in [31].

A similar conclusion was reached in discussions with the authors of further recent laser experiments [60,61], where also only the regime of nuclear spin symmetry conservation was achieved. Whether FTIR-jet spectroscopy has the sensitivity of reaching the relaxation regime is not clear, but in the laser experiments of [60,61] this might be the case in the future when using a nozzle identical to our design and under similar conditions. Indeed, an exchange of nozzles between the two setups should be feasible. That the kind of cluster formation is extremely sensitive to the exact expansion conditions has been known for some time for  $(\text{HF})_n$  clusters, where very minor changes of conditions can favour or disfavour  $(\text{HF})_2$  formation as compared to larger  $(\text{HF})_n$  clusters [40,52–55]. Irrespective of the technique used, one should point out, however, that the various spectroscopic approaches can measure only relative populations in the various rovibrational (and ortho- para-) levels, without precise information about the mechanisms by

which these arise. Thus, one should also discuss other mechanisms which might lead to populations appearing different from the standard model of nuclear spin symmetry conservation. We mention here only two of the most obvious examples. One possibility is that because of some bottlenecks, relaxation from the higher rotational levels might be very different for the ortho and para species [76]. While this seems a priori quite unlikely, arguments against this type of assumption exist in multitude and have in part been summarised before [77]. Another more plausible mechanism generating different populations would be different condensation rates of (or evaporation rates from) the ortho and the para species in the kinetics of the cluster formation (evaporation). It has notably been pointed out by Takeshi Oka that such differences exist for ortho- and para- $\text{H}_2$ . However, such a mechanism seems much less likely for  $\text{H}_2\text{O}$  because of the dipole moment and the much closer spacing of rotational levels as simple statistical capture models such as the SACM (statistical adiabatic channel model) suggest [78,79]. Also this mechanism would not explain why it would tend towards a relaxed distribution rather than some other kinetically controlled one. Also the mechanism would appear to be the same for any type of spectroscopic observation under the same clustering conditions, thus it would not explain the differences between the experiments without also assuming different clustering phenomena. A number of further mechanisms for generating non-equilibrium (non-statistical) distributions seem even less likely. Thus, the most likely explanation of the various observations (including now the observations from several laboratories) remains the mechanisms proposed by us originally, i.e. nuclear spin symmetry conservation under many conditions and possible nuclear spin symmetry relaxation in  $(\text{H}_2\text{O})_n$  under certain special clustering conditions in the experiments.

Whether the *de facto* mechanism of proton exchange in larger  $(\text{H}_2\text{O})_n$  clusters can be important could be addressed today by studies of the relevant potential hypersurfaces. While very accurate results are available for  $(\text{H}_2\text{O})_2$  [80–84], much less is known for larger clusters  $(\text{H}_2\text{O})_n$  (see, however, [85–87]). For  $(\text{HF})_n$ , this question has been systematically addressed from small to large  $n$  values [88]. We propose a similar theoretical study for  $(\text{H}_2\text{O})_n$  to address this interesting aspect of  $(\text{H}_2\text{O})_n$  kinetics in the future. The quantum relaxation mechanism in  $(\text{H}_2\text{O})_n$  could also be studied by theory, but with considerably greater difficulty. Given the possibility of preparing a beam consisting of one type of nuclear spin isomer only [89], one could also study the collisions of such a beam with  $(\text{H}_2\text{O})_n$  clusters and thus, in principle, the possibility of nuclear spin symmetry conversion in such collisions.

To summarise, we may state here, however, that our earlier results on population distributions in view of nuclear spin symmetry conservation and relaxation in (H<sub>2</sub>O) supersonic jet expansions have been confirmed and extended. The different results for different conditions in both our own experiment and in relation to other experiments have as most likely explanation the different clustering conditions in (H<sub>2</sub>O)<sub>n</sub> clusters in various experiments including cluster sizes and degree of excitation. O<sub>2</sub> (<sup>3</sup>Σ<sub>g</sub><sup>-</sup>) does not play a significant role for nuclear spin symmetry relaxation under these conditions. Theory can, in the future, in principle, address some of the questions concerning the detailed mechanisms involved.

## Acknowledgements

The authors gratefully acknowledge fruitful discussions with Veronika Horka Zelenkova, Ondrej Votava (also during a seminar at ETH Zurich), Frédéric Merkt, Jeremy Richardson and Georg Seyfang as well as discussions and correspondence with Takeshi Oka. The authors also enjoyed many years of fruitful interactions with Michel Herman on high-resolution molecular spectroscopy in general and of supersonic jets in particular. This paper is thus justly dedicated to him.

## Disclosure statement

No potential conflict of interest was reported by the authors.

## Funding

Our work was supported financially by the Schweizerischer Nationalfonds zur Förderung der Wissenschaftlichen Forschung, by an Advanced Grant of the European Research Council, ERC, as well as the ETH Zurich (Laboratory for Physical Chemistry).

## References

- [1] K.F. Bonhoeffer and P. Harteck, *Naturwiss.* **17**, 182 (1929).
- [2] R.L. Redington and D.L. Milligan, *J. Chem. Phys.* **37**, 2162 (1962).
- [3] R. Mecke, *Naturwiss.* **20**, 657 (1932).
- [4] R. Mecke and W. Baumann, *Phys. Z.* **33**, 833 (1932).
- [5] W.F. Giauque and M.F. Ashley, *Phys. Rev.* **43**, 81 (1933).
- [6] V. Tikhonov and A. Volkov, *Science* **296**, 2363 (2002).
- [7] H.A. Weaver, M.J. Mumma and H.P. Larson, *Astron. Astrophys.* **187**, 411 (1987).
- [8] M.J. Mumma, H.A. Weaver and H.P. Larson, *Astron. Astrophys.* **187**, 419 (1987).
- [9] D.A. Neufeld and G.J. Melnick, *Astrophys. J.* **368**, 215 (1991).
- [10] J. Crovisier, K. Leech, D. Bockelée-Morvan, T.Y. Brooke, M.S. Hanner, B. Altieri, H. Uwe Keller and E. Lellouch, *Science* **275**, 1904 (1997).
- [11] Truong-Bach, R.J. Sylvester, M.J. Barlow, Nguyen-Q-Rieu, T. Lim, X.W. Liu, J.P. Baluteau, S. Deguchi, K. Justtanont and A.G.G.M. Tielens, *Astron. Astrophys.* **345**, 925 (1999).
- [12] N. Babkovskaia and J. Poutanen, *Astron. Astrophys.* **418**, 117 (2004).
- [13] H. Kawakita and H. Kobayashi, *Astrophys. J.* **693**, 388 (2009).
- [14] S. Albert, B.H. Meier, M. Quack, G. Seyfang and A. Trabesinger, *Chimia* **60**, 476 (2006).
- [15] S.L. Veber, E.G. Bagryanskaya and P.L. Chapovsky, *J. Exp. Theor. Phys.* **102**, 76 (2006).
- [16] P. Cacciani, J. Cosléou and M. Khelkhal, *Phys. Rev. A* **85**, 02521 (2012).
- [17] L. Abouaf-Marguin, A.-M. Vasserot, C. Pardanaud and X. Michaut, *Chem. Phys. Lett.* **447**, 232 (2007).
- [18] L. Abouaf-Marguin, A.-M. Vasserot, C. Pardanaud, J. Stienlet and X. Michaut, *Chem. Phys. Lett.* **454**, 61 (2008).
- [19] C. Pardanaud, A.-M. Vasserot, X. Michaut and L. Abouaf-Marguin, *J. Mol. Struct.* **873**, 181 (2008).
- [20] L. Abouaf-Marguin, A.-M. Vasserot and C. Pardanaud, *J. Chem. Phys.* **130**, 054503 (2009).
- [21] L. Abouaf-Marguin, A.-M. Vasserot, C. Pardanaud and X. Michaut, *Chem. Phys. Lett.* **480**, 82 (2009).
- [22] E. Wigner, *Z. Physik Chem. B* **23**, 28 (1933).
- [23] P.L. Chapovsky, *Chem. Phys. Lett.* **254**, 1 (1996).
- [24] H.H. Limbach, G. Buntkowsky, J. Matthes, S. Grüdemann and T. Pery, *Chem. Phys. Chem.* **7**, 551 (2006).
- [25] R.F.J. Curl, J.V.V. Kasper and K.S. Pitzer, *J. Chem. Phys.* **46**, 3220 (1967).
- [26] A. Miani and J. Tennyson, *J. Chem. Phys.* **120**, 2732 (2004).
- [27] C. Manca Tanner, M. Quack and D. Schmidiger, *Faraday Discuss.* **150**, 118 (2011).
- [28] C. Manca Tanner, M. Quack and D. Schmidiger, *J. Phys. Chem. A* **117**, 10105 (2013).
- [29] M. Quack, *Mol. Phys.* **34**, 477 (1977).
- [30] C. Manca Tanner, Invited talk at the 23rd Colloquium on High Resolution Molecular Spectroscopy, Budapest, August 25–30, 2013.
- [31] R. Georges, X. Michaut, A. Moudens, M. Goubet, O. Pirali, P. Soulard, P. Asselin, T. Huet, P. Roy, M. Fournier and A. Vigasin, *J. Phys. Chem. A* **121**, 7455 (2017).
- [32] A. Amrein, M. Quack and U. Schmitt, *J. Phys. Chem.* **92**, 5455 (1988).
- [33] M. Snels, V. Horká-Zelenková, H. Hollenstein and M. Quack, in *Handbook of High-Resolution Spectroscopy, Volume 2*, edited by M. Quack and F. Merkt (Wiley, Chichester, 2011), Chapter High-resolution FTIR and Diode Laser Spectroscopy of Supersonic Jets, pp. 1021–1067.
- [34] N. Suas-David, T. Vanfleteren, T. Földes, S. Kassi, R. Georges and M. Herman, *J. Phys. Chem. A* **119**, 10022 (2015).
- [35] T. Földes, T. Vanfleteren and M. Herman, *J. Chem. Phys.* **141**, 111103 (2014).
- [36] M. Herman, K. Didriche, D. Hurtmans, B. Kizil, P. Macko, A. Rizopoulos and P. Van Poucke, *Mol. Phys.* **105**, 815 (2007).
- [37] K. Didriche, T. Földes, C. Lauzin, D. Golebiowski, J. Lievin and M. Herman, *Mol. Phys.* **110**, 2781 (2012).
- [38] M. Herman, R. Georges, M. Hepp and D. Hurtmans, *Int. Rev. Phys. Chem.* **19**, 277 (2000).
- [39] C. Manca Tanner and M. Quack, *Mol. Phys.* **110**, 2111 (2012).
- [40] M. Hippler, M. Oeltjen and M. Quack, *J. Phys. Chem. A* **111**, 12659 (2007).

- [41] C. Manca and M. Quack, Dynamics in the hydrogen bonded systems (HF)<sub>2</sub> and HFDF studied by means of cw-CRD spectroscopy, in *Proceedings of the 16th Symposium on Atomic and Surface Physics and Related Topics, Les Diablerets, Switzerland, 20. - 25.1.2008*, edited by R.D. Beck, M. Drabbels and T.R. Rizzo (Innsbruck University Press, ISBN 978-902571-31-1: Innsbruck, 2008), p. 170.
- [42] M. Hippler and M. Quack, *J. Chem. Phys.* **116**, 6045 (2002).
- [43] Y. He, M. Hippler and M. Quack, *Chem. Phys. Lett.* **289**, 527 (1998).
- [44] M. Hippler and M. Quack, *Chem. Phys. Lett.* **314**, 273 (1999).
- [45] Z. Bjelobrk, C. Manca Tanner and M. Quack, *Z. Physik. Chem.* **229**, 1575 (2015).
- [46] T. Oka, *Adv. Atom. Mol. Phys.* **9**, 127 (1973).
- [47] T. Oka, in *Handbook of High-Resolution Spectroscopy, Volume 1*, edited by M. Quack and F. Merkt (Wiley, Chichester, 2011), Chapter Orders of Magnitude and Symmetry in Molecular Spectroscopy, pp. 633–658.
- [48] M. Quack, in *Handbook of High-Resolution Spectroscopy, Volume 1*, edited by M. Quack and F. Merkt (Wiley, Chichester, 2011), Chapter Fundamental Symmetries and Symmetry Violations from High-resolution Spectroscopy, pp. 659–722.
- [49] J.B. Paul, C.P. Collier, R.J. Saykally, J.J. Scherer and A. O’Keefe, *J. Phys. Chem. A* **101**, 5211 (1997).
- [50] U. Buck and F. Huisken, *Chem. Rev.* **100**, 3863 (2000).
- [51] D. Nesbitt, T. Häber and M.A. Suhm, *Faraday Discuss.* **118**, 304 (2001).
- [52] M. Quack, U. Schmitt and M. Suhm, *Chem. Phys. Lett.* **208**, 446 (1993).
- [53] M. Quack, U. Schmitt and M.A. Suhm, *Chem. Phys. Lett.* **269**, 29 (1997).
- [54] M. Quack, U. Schmitt and M.A. Suhm, *J. Aerosol Sci.* **28** (Suppl. 1), S363 (1997).
- [55] D. Luckhaus, M. Quack, U. Schmitt and M. Suhm, *Ber. Bunsenges. Phys. Chem.* **99**, 457 (1995).
- [56] P.L. Chapovsky and L.J.F. Hermans, *Ann. Rev. Phys. Chem.* **50**, 315 (1999).
- [57] P.L. Chapovsky, *J. Phys. B* **33**, 1001 (2000).
- [58] P.L. Chapovsky, J. Cosléou, F. Herlemont, M. Khelkhal and J. Legrand, *Chem. Phys. Lett.* **322**, 424 (2000).
- [59] W.B. Chapman, A. Schiffman, J.M. Hutson and D.J. Nesbitt, *J. Chem. Phys.* **105**, 3497 (1996).
- [60] O. Votava, *Seminar at ETH Zurich* (2014).
- [61] O. Votava, V. Zelenkova and J. Rakovsky, *Proceeding in XXIst Symposium on Atomic, Cluster and Surface Physics 2018 (SASP 2018) February 11–16, 2018 Obergurgl, Austria, 2018*, 196.
- [62] A. Farkas, *Orthohydrogen, Parahydrogen and Heavy Hydrogen* (Cambridge University Press, Cambridge, 1935).
- [63] B. Nagels, P. Bakker, L. Hermans and P.L. Chapovsky, *Chem. Phys. Lett.* **294**, 387 (1998).
- [64] M. Quack, *Ann. Rev. Phys. Chem.* **41**, 839 (1990).
- [65] M.P. Sinha, A. Schultz and R.N. Zare, *J. Chem. Phys.* **58**, 549 (1973).
- [66] R.E. Smalley, L. Wharton and D.H. Levy, *Accounts Chem. Res.* **10**, 139 (1977).
- [67] G. Lujks, S. Stolte and J. Reuss, *J. Chem. Phys.* **62**, 217 (1981).
- [68] H.R. Dübal, M. Quack and U. Schmitt, *Chimia* **38**, 438 (1984).
- [69] A. Amrein, M. Quack and U. Schmitt, *Mol. Phys.* **60**, 237 (1987).
- [70] A. Amrein, D. Luckhaus, F. Merkt and M. Quack, *Chem. Phys. Lett.* **152**, 275 (1988).
- [71] A. Beil, D. Luckhaus, R. Marquardt and M. Quack, *Faraday Discuss.* **99**, 49 (1994).
- [72] M. Snels, A. Beil, H. Hollenstein, M. Quack, U. Schmitt and F. D’Amato, *J. Chem. Phys.* **103**, 8846 (1995).
- [73] A. Bauder, A. Beil, D. Luckhaus, F. Müller and M. Quack, *J. Chem. Phys.* **106**, 7558 (1997).
- [74] M. Herman, in *Handbook of High-Resolution Spectroscopy, Volume 3*, edited by M. Quack and F. Merkt (Wiley, Chichester, 2011), Chapter High Resolution Spectroscopy of Acetylene.
- [75] M. Herman, K. Didriche, A. Rizopoulos and D. Hurtmans, *Chem. Phys. Lett.* **414**, 282 (2005).
- [76] D. Nesbitt, *Faraday Discuss.* **150**, 120 (2011).
- [77] C. Manca Tanner, M. Quack and D. Schmidiger, *Faraday Discuss.* **150**, 121 (2011).
- [78] M. Quack and J. Troe, *Ber. Bunsenges. Phys. Chem.* **79**, 170 (1975).
- [79] M. Quack and J. Troe, in *Encyclopedia of Computational Chemistry, Volume 4* (Wiley, New York, 1998), Chapter Statistical Adiabatic Channel Model, pp. 2708–2726.
- [80] R.S. Fellers, C. Leforestier, L.B. Braly, M.G. Brown and R.J. Saykally, *Science* **284**, 945 (1999).
- [81] C. Leforestier, L.B. Braly, K. Liu, M.J. Elrod and R.J. Saykally, *J. Chem. Phys.* **106**, 8527 (2001).
- [82] N. Goldman, R.S. Fellers, C. Leforestier and R.J. Saykally, *J. Phys. Chem. A* **105**, 515 (2001).
- [83] F.N. Keutsch, L.B. Braly, M.G. Brown, H.A. Harker, P.B. Petersen, C. Leforestier and R.J. Saykally, *J. Chem. Phys.* **119**, 8927 (2003).
- [84] G.S. Tschumper, M.L. Leininger, B.C. Hoffman, E.F. Valeev, H.F. Schaefer and M. Quack, *J. Chem. Phys.* **116**, 690 (2002).
- [85] J.O. Richardson, D.J. Wales, S.C. Althorpe, R.P. McLaughlin, M.R. Viant, O. Shih and R.J. Saykally, *J. Phys. Chem A* **117**, 6960 (2013).
- [86] J.O. Richardson, C. Perez, S. Lobsiger, A.A. Reid, B. Temeslo, G.C. Shields, Z. Kisiel, D.J. Wales, B.H. Pate and S.C. Althorpe, *Science* **351**, 1310 (2016).
- [87] J.C. Howard and G.S. Tschumper, *J. Chem. Theory Comput.* **11**, 2126 (2015).
- [88] W. Klopper, M. Quack and M. Suhm, *Mol. Phys.* **94**, 105 (1998).
- [89] D.A. Horke, Y.P. Chang, K. Dlukolecki and J. Küpper, *Angew. Chem. Int. Ed.* **53**, 11965 (2014).